Journal of Hazardous Materials 424 (2022) 127318

Contents lists available at ScienceDirect

Journal of Hazardous Materials

journal homepage: www.elsevier.com/locate/jhazmat

Chlorpyrifos triggers epithelioma papulosum cyprini cell pyroptosis via miR-124-3p/CAPN1 axis

Zhiying Miao [a], Zhiruo Miao [b], Xiaohua Teng [a,*], Shiwen Xu [b,*]

[a] College of Animal Science and Technology, Northeast Agricultural University, Harbin 150030, People's Republic of China
[b] College of Veterinary Medicine, Northeast Agricultural University, Harbin 150030, People's Republic of China

ARTICLE INFO

Editor: Dr. S Nan

Keywords:
Organophosphorus pesticides
Pyroptosis
NLRP3 inflammasome
Calpain1
MicroRNA-124-3p

ABSTRACT

Chlorpyrifos (CPF), a widely used organophosphorus pesticide has caused water pollution, threatening aquatic organisms. MicroRNAs (miRNAs) highly conserved noncoding RNAs, that regulate various cell death processes, including pyroptosis. To investigate the effect of CPF exposure on epithelioma papulosum cyprini (EPC) cell pyroptosis and the role of the miR-124-3p/CAPN1 axis, we established miR-124 overexpression and inhibition EPC cell models of CPF exposure. The target of the miR-124-3p/CAPN1 axis was primarily confirmed by the double luciferase reporter assay. Pyroptosis was demonstrated to occur in CPF-exposed EPC cells and was accompanied by mitochondrial membrane potential depletion, ROS level elevation and pyroptotic indicator expression upregulation. PD150606 was supplied as a CAPN1 inhibitor, alleviating CPF-induced mitochondrial dysfunction, and alleviating the increased expression of NLRP3, CASP1, IL1β and GSDMD. In conclusion, CPF induces pyroptosis by regulating the miR-124-3p/CAPN1 axis. This study enriches the cytotoxicity study of CPF, and provides new theoretical fundamentals for exploration of miRNA and its target protein response to water contaminants.

1. Introduction

Organophosphorus pesticides (OPs.) as a general classification of organic ester compounds comprised of phosphorus atoms, have been extensively used as insecticides, fungicides and herbicides for five decades for the agricultural control of insect pests, and they make up approximately 38% of the total pesticides used worldwide (Pundir et al., 2019). The broad utilization of OP contaminates water resources, crops and processed food, thereby harming various organisms including poultry, fish and humans (Randriamboavonjy et al., 2019). Chlorpyrifos (CPF) is a common OP that is controversial due to its extensive consumption, environmental implications and high health risks. In 2015, over two-hundred-thousand (200,000) tons of CPF were applied worldwide (Huang et al., 2020). Precipitation runoff, irrigation water runoff, stormwater outflow and leakage accidents all contribute to CPF induced aqueous pollution. The CPF leakage accident that occurred in the Bay of Cartagena, Colombia causing 17 t of fish to died (Cowgill et al., 1991). Approximately 9% of over ten thousand streams in the United States have detectable CPF with a maximum concentration of 3.96 μg/L (Williams et al., 2014), although the benchmark concentration of CPF for freshwater fish is 0.57 μg/L (EPA, 2000). According to survey by the Pesticide Data Programs of the USA, CPF has been detected in several fruits and vegetables, such as cherry, peach, plum, bell peppers and summer squash (Pesticide Data Programs of USA, 2016). CPF residue detection in food and human blood indicated that the residue concentration of CPF in both food and human blood is beyond the human safety levels (Liao et al., 2017). Additionally, the European Food Safety Authority has documented that CPF continually exceeds the acute reference dose in various food products (Liang et al., 2019). Previous studies have reported CPF is able to mediate cytotoxicity via various mechanisms (Ojha et al., 2013; Yamada et al., 2017; Naime et al., 2020). Oxidative damage is primarily induced by the imbalance of reactive oxygen species (ROS) generation and elimination, resulting in the alteration of signalling pathways and interference with cellular metabolism (Gorrini et al., 2013), thereby further inducing systemic diseases such as inflammation and the immune response (Reuter et al., 2010). Many studies have clarified that CPF causes inflammatory damage in multiple organs including hepatic (Albasher et al., 2020), cerebral and ocular tissues (AlKahtane et al., 2020). Weis et al. (2021) declared that CPF crosses the blood-brain barrier promoting the expression of NOD-like receptor (NLR) family pyrin domain-containing 3 (NLRP3) and interleukin (IL)1β in microglial cells. Previous studies

* Corresponding authors.
E-mail addresses: tengxiaohua@neau.edu.cn (X. Teng), shiwenxu@neau.edu.cn (S. Xu).

https://doi.org/10.1016/j.jhazmat.2021.127318
Received 6 July 2021; Received in revised form 8 September 2021; Accepted 19 September 2021
Available online 24 September 2021

have shown that CPF causes pyroptosis in human keratinocytes (Jang et al., 2015) and neuroblastoma cells (Zhao et al., 2019). The relevance of CPF as a water contaminant to inflammation and immunodepression in aquatic organisms has been verified. Karbalaei et al. (2021) revealed that CPF induced histopathological inflammatory lesions on the gills of *Oncorhynchus mykiss*. Dawood et al. (2020) confirmed that CPF induced inflammation and immunosuppression and histopathological changes in Nile tilapia. Zhang et al. (2017a) revealed that CPF exposure results in oxidative stress and immune responses in common carp (*Cyprinus carpoi* L.).

Calpains are a family of calcium-dependent thiol proteases, containing 15 isoforms that regulate the proteolysis of various substrates, and they are involved in numerous cellular processes including cellular signallings, cytoskeletal/membrane attachment remodeling and cell survival (Storr et al., 2011). Reduction of calpain activity are accompanied by dyshomeostasis of calcium ions in response to tissue damage induced by myocardial infarction, apoplexy and cerebral trauma (Goll et al., 2003). Calpain1 (CAPN1) as the primary isoform of calpains, requires calcium ion levels and a neutral pH in vitro for its activity and it is involved in the degradation of cell structural proteins (Yue et al., 2019). As concluded by Tangmansakulchai et al. (2016), CAPN1 triggers mitochondrial fission by activating calcineurin which correlates with the phosphorylation of dynamin-related protein 1 (DRP1). Mitochondrial fusion is modulated by optic atrophy 1 (OPA1), and OPA1 suppression results in mitochondrial fission, fragmentation and even death (Guan et al., 2019). A recent study by Tong et al. (2020) reported that homeostasis of mitochondrial fission/fusion plays an essential role in mitochondrial dysfunction protection, and DRP1 is crucial for impaired mitochondrial isolation and degradation. Furthermore, numerous studies have raised concerns about CAPN1 related to the activation of inflammasomes (Yue et al., 2019) (Yu et al., 2020). A study by Zhang et al. (2018) verified that calpain activation was associated with the release of caspase1 (CASP1) from the actin cytoskeleton and flightless-1, and that the released CASP1was involved in forming the NLRP3 inflammasome. Yue et al. (2019) reported that calpain mediated NLRP3 inflammasome assembly induces myocardial ischaemia-reperfusion injury. Additionally, calpain participated in myocarditis induced by coxsackievirus B3 through the NLRP3 inflammasome/CASP1 pathway. NLRP3 inflammasomes are large multiprotein complexes of CASP1, ASC as the adaptor protein, and NLRP3, which are closely associated with cell pyroptosis. The activation of CASP1, as an inflammatory caspase, governs gasdermin D (GSDMD) cleavage, and results in IL1β and IL18 maturation (He et al., 2015). Then proinflammatory factors, including IL1β and IL18, are released from pyroptotic cells, resulting in GSDMD-dependent inflammatory response (Bergsbaken et al., 2009; Broz et al., 2020). Activation of NLRP3 inflammasome stimulated by external stimuli, contributes to pyroptosis. Song et al. (2021) reported that hydrogen sulphide causes pyroptosis in broiler trachea via the NLRP3 inflammasome pathway. Consistently, cell pyroptosis was found in molybdenum and cadmium cotreated duck renal tubular epithelial cells by activating the NLRP3 inflammasome (Zhang et al., 2021). Wu et al. (2018) reported that nicotine triggers pyroptosis through ROS/NLRP3 in endothelial cells. Li et al. (2019) verified that lipopolysaccharide (LPS) causes inflammation and pyroptosis via the NLRP3 signalling pathway.

MicroRNAs (miRNAs) are small and highly conserved noncoding RNAs that regulate the deadenylation, degradation or translation of mRNA, and fundamentally modulate various cell processes (Kanagaraj et al., 2014). Accordingly, adjusting of specific miRNAs provides distant insight into the mechanistic exploration of diseases. MiR-124 has been shown to contribute to CAPN1 regulation in murine neurons (Kanagaraj et al., 2014) and human neural cells (Zhou et al., 2019). However, the relationship between miR-124 and CAPN1 in fish is unconfirmed, and whether CPF induces cell pyroptosis in fish and the roles of miR-124/CAPN1 in the cytotoxicity of CPF are still obscured. We used epithelioma papulosum cyprini (EPC) cells as the research object in the present study, and verified the binding of 124–3p to CAPN1 by a double luciferase reporter assay. Accordingly, miR-124 NC, mimic and inhibitor cell models were established and treated with CPF and PD150606 (noncompetitive calpain inhibitor), respectively, to stimulate the cells. JC-1 staining, ROS assay kits and western blotting were performed to confirm the mitochondrial functional alterations. Immunofluorescence, RT-PCR and western blotting were subsequently applied to monitor the effects of CPF on the expression of the pyroptosis-related genes. We designed this study to demonstrate that CPF induced EPC cell pyroptosis via regulating the miR-124-3p target, CAPN1 expression. These results provide new evidence to further elucidate the toxicological mechanism of CPF.

2. Material and methods

2.1. Cell modes establishment

Frozen EPCs were obtained from laboratory cell storage containers. The frozen cell tubes were immediately sunk in 37 ℃ sterile water bath. The melted cell suspension was transferred into cell culture medium mixture of 89% M199 cell medium (HyClone, USA), 10% foetal bovine serum (Biological Industries, Israel) and 1% penicillin-streptomycin (Sigma-Aldrich, USA). The cells were incubated in a 25 cm^2 culture flask in a 27 ℃ automatic incubator with 95% air and 5% CO_2. To confirm the effects of CPF on EPCs, we collected the cells by using trypsin digestion solution (0.25%, Biosharp, China). Cell Counting Kit-8 (CCK-8, Saint Biotec, China) was used to detect CPF-induced cytotoxicity. The EPCs were treated with various concentrations of CPF (0, 1, 3, 5, 7, 9, 11, or 13 μM) for 24 h in 96-well plates. Fresh culture medium containing 10% CCK-8 was added to replace the CPF medium for 1 h, and then a Cytation5 imaging plate reader (Biotek Instrument, USA) was used to detect the absorbance at 450 nm. As shown in Supplementary Fig. 1, we treated the cells with 0, 3, 5, and 7 μM CPF for 24 h and placed the cells in the C, L, M, and H group.

To further explore the mechanism by which miR-124 and CAPN1 target CPF-induced EPC cell cytotoxicity, we established overexpression and inhibition cell models. The cells were seeded in 6-well plates for 24 h. Subsequently, we transfected the cells with 5 μL of miR-124 mimic (20 μM, Ribobio, China), miR-124 inhibition (20 μM, Ribobio, China) or miR-124 negative control (miR-124 NC, 50 nM, Ribobio, China) and 3 μL of Lipofectamine 2000 (Invitrogen, Thermo Fisher Scientific, USA) in 1 mL of Opti-MEM (Gibco, Thermo Fisher Scientific, USA) for 6 h. After transfection, the cell culture medium was replaced with fresh cell culture medium mixture or cell medium mixture containing 7 μM CPF or/and 50 μM PD150606 (MedChemExpress) for further incubation for 24 h. The sequence of the miR-124 mimic was 5'- UAAGGCACGCGGUGAAUGCCAA −3', and the sequence of the miR-124 inhibitor was 5'-mAmUmUmCmGmUmGmCmGmCmCmAmCmUmU-mAmCmGmGmUmU-3', and the miR-124 NC sequence was 5'-mCmUmGmCmCmUmGmUmCmUmGmUmGmCmCmUmGmC-mUmGmU-3.

2.2. Dual luciferase reporter assay

Based on the pMIR-REPORT luciferase plasmids, we constructed new vectors in this study. According to the gene sequences of CAPN1 on the NCBI website, we designed a CAPN1 3' untranslated region (3'UTR) containing the miR-124 binding site and the corresponding mutant sequences (Fig. 1**E**) were synthesized and individually cloned into the pMIR-REPORT vector (Thermo Fisher Scientific, USA) and called as CAPN1-pMIR-WT and CAPN1-pMIR-MT. The pMIR-REPORT luciferase plasmids were digested by using the restriction enzymes *Hin*dIII and *Sac*I, and gel extraction after nucleic acid electrophoresis was used to isolate the desired fragments. Then, they were connected with the designed fragments by using T4 ligase at 16 ℃ for 8 h. The vector was transformed into T1 competent cells, and after coating the plates,

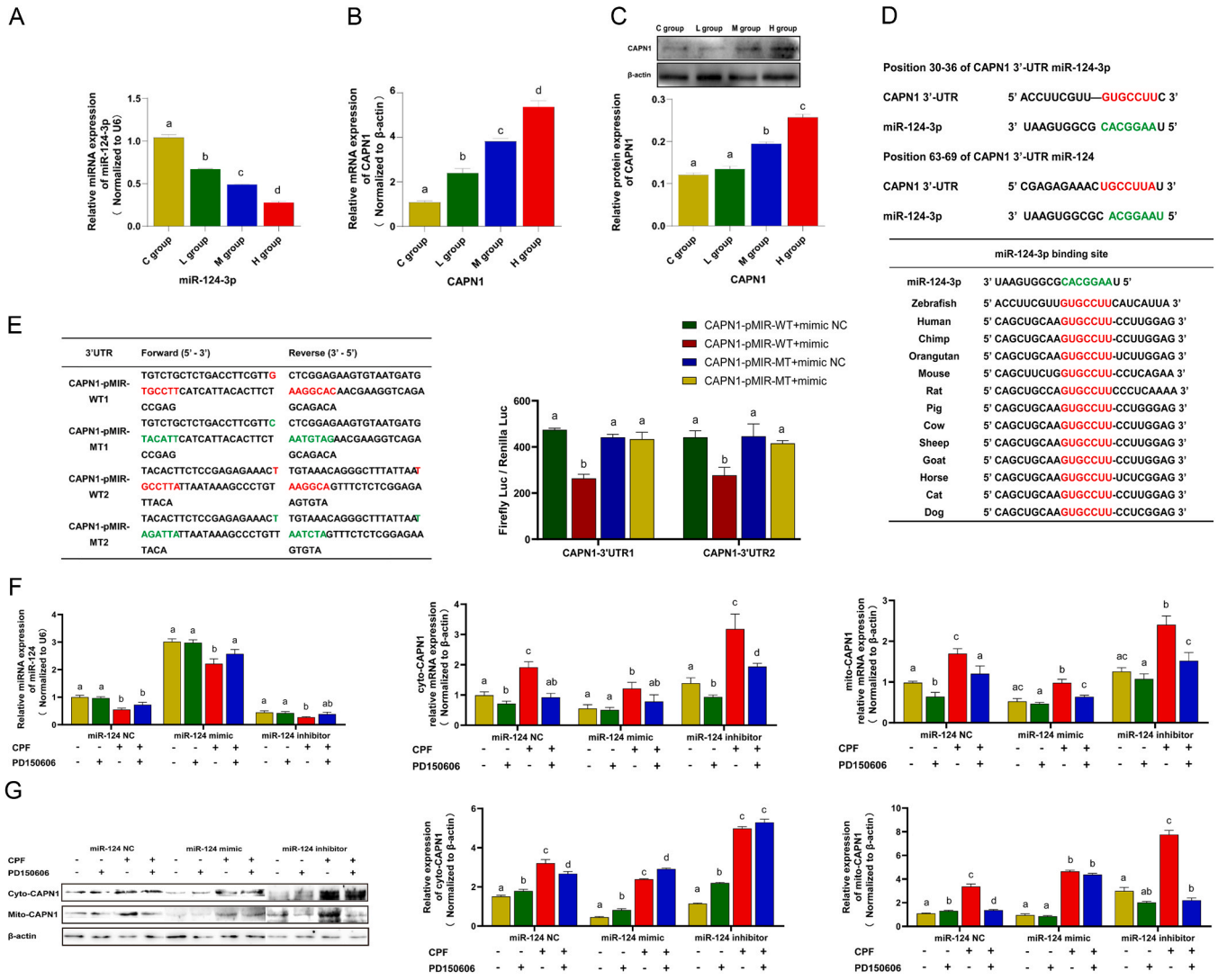

Fig. 1. Decreased miR-124-3p expression targeted CAPN1 enhancement under CPF exposure. (A) The miRNA expression of miR-124-3p under various CPF exposures. The C, L, M, and H group cells were exposed to 0, 3, 5, and 7 μM CPF, respectively. The data were analysed by one-way ANOVA, and different superscript letters display statistically significant differences ($P < 0.05$). (B-C) The mRNA and protein expression levels of CAPN1 under various CPF exposure conditions. (D) Highly conserved binding sites of miR-124-3p and CAPN1 among multiple organisms were predicted by the TargetScan website. (E) The pMIR-REPORT plasmids for the dual luciferase reporter assay. The red font indicates the target location of wild-type bases, and the green font marks mutated bases. The results are shown as firefly luciferase normalized to Renilla luciferase as Luc/R-luc. The data were analysed by one-way ANOVA, and different superscript letters display statistically significant differences ($P < 0.05$). (F) The miRNA and mRNA expression levels of miR-124, cytoplasmic (cyto)-CAPN1 and mitochondrial (mito-CAPN1). The EPCs were incubated in 6-well plates and transfected with miR-124 mimic, miR-124 inhibition or miR-124 NC for 6 h. The medium was replaced with fresh culture medium for 24 h, and the medium was changed to fresh cell culture medium or cell medium containing 7 μM CPF and/or 50 μM PD150606 (CAPN1 inhibitor) for 24 h. The data were analysed by two-way ANOVA, and different superscript letters display statistically significant differences ($P < 0.05$). (G) The protein levels of cyto-CAPN1 and mito-CAPN1 in each group of cells.

colonies were selected, amplified, and plasmid extraction was performed. The recombinant plasmid was stored at −20 ℃ for later cell transfection. EPCs were cotransfected with the phRL-TK vector, miR-124 mimic, and designed vectors using Opti-MEM containing Lipofectamine 2000 reagent. After transfection for 6 h, the medium was replaced with fresh medium for 24 h, and then the cells were treated with or without 7 μM CPF and/or 50 μM PD150606. The cellular protein lysates were assayed using the DualGLO® Luciferase Assay System (Promega, USA). Firefly luciferase activity was normalized to Renilla luciferase activity for each group.

2.3. Mitochondrial functional assessment

To identify CPF induced functional alterations of the mitochondria, a JC-1 assay kit (Shanghai Beyotime Biotechnology, China) and a ROS assay kit (Nanjing Jianchang Bioengineering Research Institute, China) were used in this study to identify the mitochondrial membrane potential (MMP) and intracellular and mitochondrial ROS levels. In accordance with the instruction manual, the cells were pretreated and incubated in 6-well plates, and then after loading for 20 min with JC-1 working solution, which was comprised of 50 μL JC-1 (200X), 8 mL ultra-pure water and 2 mL JC-1 buffer solution (5X), they were washed twice with JC-1 buffer solution (1X). Fluorescence microscopy (Thermo Fisher Scientific, USA) was used to observe the emission of green JC-1 monomers and red JC-1 aggregates at fluorescence emission wavelengths of 530 and 590 nm, respectively.

To determine the intracellular and mitochondrial ROS levels, mitochondria were isolated with a cell mitochondria isolation kit (Shanghai Beyotime Biotechnology, China). The pretreated cells were incubated in culture flasks, collected by using trypsin digestion solution and

centrifuged at 800 rpm for 5 min. The cells were resuspended in cold mitochondrial isolation reagent containing 1 mM PMSF and placed in an ice bath for 15 min. Then, they were homogenized with a glass homogenizer, and t centrifuged at 4 °C at 2000 rpm for 10 min. The supernatant was obtained and was put into a new EP tube. The EP tube was centrifuged at 4 °C at 12,000 rpm for 10 min. The obtained sediment was the isolated mitochondria that was used for subsequent experiments. Staining medium containing 10 μM 2,7-dichlorofuresc in diacetate (DCFH-DA) was added to each group cells and the mitochondria were isolated after 45 min. The intracellular ROS levels were observed with a fluorescence microscop (Thermo Fisher Scientific, USA), and the mitochondrial ROS levels were detected with a fluorospectrophotometer.

2.4. Pyroptotic cell staining

To observe the pyroptosis that occurred in the groups, Hoechst, Annexin V-FITC and PI Hoechst staining mixtures were applied to stain pyroptotic cells. The transfected cells were seeded in 6- well plates, and treated with or without 7 μM CPF. Hoechst staining solution (1 μg/mL, Shanghai Beyotime Biotechnology, China) was applied to the cells for 30 min in an ice bath, and after rinsing with PBS once, 1 mL staining mixture comprised of 800 μL buffer solution, 10 μL Annexin V-FITC and 10 μL PI (KeyGEN BioTECH, China) was added for 20 min. Then, a fluorescence microscope (Thermo Fisher Scientific, USA) was used to observe pyroptosis.

2.5. Immunofluorescence

The pretreated cells were incubated in 6-well plates, rinsed with PBS, and fixed in 4% paraformaldehyde at 4 °C overnight. They were permeabilized for 10–15 min with TBSTx containing 0.1% Triton X-100 in Tris-buffered saline (TBS), and blocked with 5% bovine serum albumin (BSA, BioFroxx, Germany) in TBSTx for 60 min. Anti-NLRP3 primary antibody (1:100, Wanleibio, China), anti-CASP1 primary antibody (1:100, Wanleibio, China) and GSDMDS (1:200, ABclonal Biotechnology) were diluted with primary antibody diluent (Shanghai Beyotime Biotechnology, China) and incubated at 4 °C overnight. After washing with TBSTx for 15 min, Alexa Fluro 488 goat anti-rabbit IgG (1:1000, Biodragon Immunotechoology, China) and DyLight 594 goat anti-rabbit IgG (1:1000, Biodragon Immunotechoology, China) secondary antibodies were applied for 120 min at room temperature. After rinsing with TBSTx for 15 min, DAPI (Shanghai Beyotime Biotechnology, China) was used to stain the cell nucleus for 5 min and a fluorescence microscope (Thermo Fisher Scientific, USA) was used to image the samples.

2.6. Quantitative real-time PCR (qRT-PCR)

TRIzol reagent (product No.15596–018, Life Technologies, USA) was used to extract the total RNA from each group. The pretreated cells in each group were incubated in 6-well plates and scraped to collect the cells in 1.5 mL EP tubes without RNase on ice after adding 500 μL TRIzol. After vigorous vortexing and being left to stand for 10 min, we added 400 μL chloroform for 5 min. Then, they were centrifuged at 13,000 rpm for 15 min, we removed the supernatant and added an equal volume of cold isopropyl alcohol for 10 min. The solution was centrifuged at 12,000 rpm for 15 min and the supernatant was discarded. We added 1 mL of 75% ethanol to resuspend the precipitate, and centrifuged it at 7500 rpm for 5 min at 4 ℃, discarded the supernatant and dried the pellet for 5–8 min. Then we used RNase-free water to dissolve the precipitation and stored it at −20 ℃ for subsequent study. The Tiangen miRNA cDNA Synthesis kits (Tiangen Biotech, China) and the BioRT mRNA cDNA Synthesis kits (Bioer Technology, China) were applied following the manufacturer's instructions for reverse transcription in a volume of 40 μL (containing 2 μg of the total RNA). QuantStudio 3 and Tiangen miRNA qPCR kits (Tiangen Biotech, China) or BioRT RT-PCR kits (Bioer Technology, China) were used in the qRT-PCR process. The reaction system comprised 0.3 μL of forward and reverse primers, 1 μL of diluted cDNA, 3.4 μL of sterile distilled water, and 5 μL of SYBR green mix. The reaction system for miRNA was comprised of 0.2 μL of forward and reverse primers, 1 μL of diluted miRNA cDNA, 3.6 μL of sterile distilled water, and 5 μL of 2 × miRcut microRNA premix. The primers for the miRNA and mRNA of genes were synthesized as shown in Table 1. U6 and β-actin were used as internal references.The $2^{-\Delta\Delta Ct}$ method was used to calculate the relative miRNA and mRNA abundances.

2.7. Western blot analysis

PMSF was used during the extraction of protein in this study. One microliter of PMSF (Shanghai Beyotime Biotechnology, China) was added to 100 μL of cell lysate (Shanghai Beyotime Biotechnology, China) and incubated with the cells for 30 min in an ice bath. The supernatant obtained after centrifugation (12,000 rpm) at 4 ℃ for 25 min, and it was boiled for 10 min after adding SDS-PAGE loading buffer (Shanghai Beyotime Biotechnology, China). The proteins were separated on 12% SDS-PAGE, and the proteins were transferred cto PVDF membranes under 200 mA in Tris-glycine buffer for 60–130 min. Five percent skim milk was applied to block the membrane at 37 °C for 120 min, and then it was incubated in diluted primary antibody at 4 °C overnight. BSA (5%; BioFroxx, Germany) was used to dilute the antibody, and the dilution factors of the primary antibodies used in this study are listed in Table 2. Secondary antibodies against rabbit IgG (1:10000, Immunoway, China) were used to detect the bound antibodies for 120 min. A chemiluminescence system (Applygen Technologies, China) and X-ray films (TransGern Biotech, China) were used to analyse the protein bands and normalize them against β-actin. ImageJ software (National Institutes of Health) was applied to quantify the intensity of the bands.

2.8. Statistical processing

The data were processed with GraphPad Prism (version 8.2, GraphPad Software, USA) and analysed by Shapiro–Wilk for normality, and these data passed the normality test (alpha=0.05). Student's *t*-test, one-way or two-way ANOVA with Tukey's multiple comparison test were performed, and the data are expressed as the mean ± standard deviation, and statistically significant differences were considered at $P < 0.05$.

Table 1
The primer sequences synthesis for qRT-PCR.

	Sequence (5' - 3')
miR-124	TAAGGCACGCGGTGAATGCCAA
U6	CTCGCTTCGGCAGCACA
CAPN1	Forward:ACCAATTTGTTCCTTCTGATCCTCCTC
	Reverse: AAACACTCTGCGAAACTGCCTCTC
DRP1	Forward:GGTCACAGAGCAGTGGAAAGAGTTC
	Reverse: GGTCACAGAGCAGTGGAAAGAGTTC
OPA1	Forward:GGACACTTGGCACCAACTCTATCG
	Reverse: ATCCTCCAGAACAGAACCACATCATTG
NLRP3	Forward:GCTCATGTTCTGCTGTGTCTCTCC
	Reverse: GGATGATCTGGATATGGCTGCTTCTG
CASP1	Forward:CTCCGAACTGTGCTGGATTGAAGG
	Reverse: GCTCTTTTGCTCTGTTGCGTCTTG
IL1β	Forward:CTTCCACCCTCACAAACACATTCAAC
	Reverse: AATATAGCGTCCAAGGCGTTCCATC
β-actin	Froward:GGCTCTCTTCCAGCCTTCCT
	Reverse: AGCACGGTGTTGGCATACAG

Table 2
Antibodies diluted for Western blotting.

Antibodies	Dilution ratio	Resource
CAPN1	1:500	Wanleibio, China
DRP1	1:500	Wanleibio, China
OPA1	1:2000	Laboratory made
NLRP3	1:500	Wanleibio, China
CASP1	1: 500	Wanleibio, China
IL1β	1:500	Wanleibio, China
GSDMD	1:2000	ABclonal Biotechnology
β-actin	1:1500	ABclonal Biotechonology

3. Results

3.1. miR-124-3p targets CAPN1 expression under CPF exposure

To further confirm the effects of CPF on miR-124-3p and CAPN1 in EPC cells, we detected the expression of miR-124-3p and CAPN1, as shown in Fig. 1. We found that the expression of miR-124-3p significantly ($P < 0.05$) declined in a concentration-dependent manner, and the lowest level was observed in the H group, with the highest level in the C group (Fig. 1A). In contrast, CAPN1 manifested significantly ($P < 0.05$) enhanced expression in the H group and showed an escalating trend with increasing CPF exposure (Fig. 1B-C). The predicted binding sites of miR-124-3p in CAPN1 were consistent with the highly conserved binding site of miR-124-3p, depending on TargetScan (http://www.targetscan.org/fish_62/) predications (Fig. 1D). To further verify the target binding of miR-124-3p in CAPN1, a double luciferase reporter assay was performed in this study. The results revealed a significant decrease in the fluorescence intensity of the CAPN1-pMIR-WT+mimic groups compared with the other groups (Fig. 1E), indicating that miR-124-3p interacts with CAPN1 via two predicted binding sites. PD150606, a nonpeptide and noncompetitive calpain inhibitor (Luo et al., 2015), has been applied in different cell models. Therefore, the interaction among CPF, miR-124-3p and CAPN1 depended on the expression at the miRNA, mRNA and protein levels, as shown in Fig. 1F-G. We found that CPF significantly increased the expression of cytoplasmic (cyto)-CAPN1 and mitochondrial (mito)-CAPN1 in all cell models compared with the untreated group. The addition of PD150606 significantly abolished the CPF-mediated high expression of CAPN1. Consistent with the above findings, we explored three cell models, and we found higher CAPN1 expression in the miR-124 inhibitor group than in the mimic group, which demonstrated that CPF enhanced CAPN1 expression by regulating miR-124-3p.

3.2. CPF triggered mitochondrial dysfunction via miR-124-3p/CAPN1 axis

To further understand the effects of CPF on mitochondrial functional conditions, MMP status, mitochondrial fusion/fission homeostasis and ROS levels were detected in this study, as shown in Fig. 2. Because MMP loss has been considered an early crucial event in mitochondrial dysfunction, JC-1 assay kits were used to monitor the alteration of MMP in this study. The flow cytometry results showed that MMP in the miR-124 NC, mimic and inhibitor groups shifted from Q2 to Q4 in comparison with the untreated group (Fig. 2A), which illuminated that ΔΨm was suppressed by CPF exposure. Additionally, a higher ΔΨm was observed in the miR-124 mimic group untreated with CPFs than in the

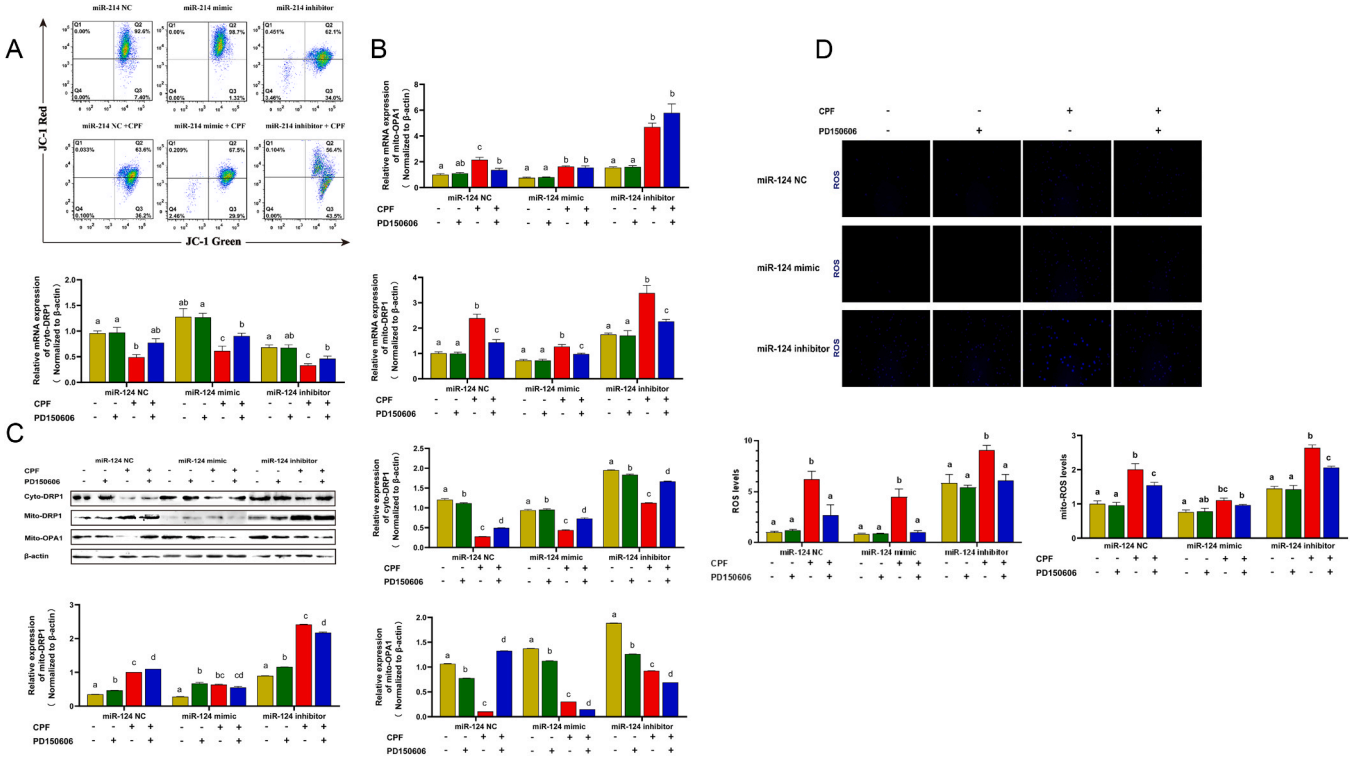

Fig. 2. CPF induced mitochondrial dysfunction and ROS overproduction via miR-124-3p/CAPN1 axis. (A) The mitochondrial membrane potential (MMP) status of the groups was detected by JC-1 assay kits. JC-1 aggregates were formed in the matrix of mitochondria as a result of higher MMP and they emitted red fluorescence. In contrast, JC-1 could not aggregate under lower MMP and existed as a monomer, which emitted green fluorescence. (B) The mRNA expression of mito-OPA1, cyto-DRP1 and mito-DRP1 in the miR-124 mimic, miR-124 inhibition and miR-124 NC cell models with or without 7 μM CPF and/or 50 μM PD150606 treatment. (C) The protein levels of mito-OPA1, cyto-DRP1, mito-DRP1 and mito-OPA1 in each group of cells. (D) Intracellular and mitochondrial ROS levels were determined by DCFH-DA staining. The intracellular ROS levels were detected by fluorescence microscopy, and the mitochondrial ROS levels were assessed with a fluorospectrophotometer. The intensity of the fluorescence, which indicates the ROS levels, was measured from three randomly chosen fields of view. The data were analysed by two-way ANOVA, and different superscript letters display statistically significant differences ($P < 0.05$).

miR-124 NC group, but the difference was negligible under CPF exposure. However, ΔΨm was decreased in the miR-124 inhibitor group under both untreated and treated CPF exposure. Taken together, CPF induced MMP depletion by inhibiting miR-124 expression to target CAPN1 elevation. Mitochondrial fragmentation is associated with impaired respiration, resulting in reduced ΔΨm (Osellame et al., 2013). To verify whether CPF-induced MMP depletion is related to mitochondrial fusion/fission dynamics, we detected the expression of related genes, such as DRP1 and OPA1 (Fig. 2B-C). The expression of cyto-DRP1 significantly ($P < 0.05$) declined under CPF treatment, and the addition of PD150606 significantly ($P < 0.05$) rescued CPF-induced depression. However, the opposite alterations were observed in mito-DRP1 expression, as PD150606 significantly ($P < 0.05$) alleviated the CPF-mediated upregulation of mito-DRP1, which confirmed that DRP1 translocated from the cytoplasm into the mitochondria to enhance mitochondrial fragmentation. Interestingly, mito-OPA1 showed slightly stronger expression in the miR-124 inhibitor model under combined treatment with CPF and PD150606 than in the CPF-treated group. Subsequently, the intracellular and mitochondrial ROS levels of each group were tested with ROS assay kits (Fig. 2D). The results clearly showed that CPF induced ROS in all cell models and that ROS levels in the miR-124 inhibitor group were much higher than those in the NC and mimic groups, which indicates that inhibition of miR-124-3p enhanced mitochondrial fragmentation and resulted in ROS overproduction. Supplementation with PD150606 played a significant role in mitigating CPF-induced intracellular ROS generation. Therefore, CPF induced mitochondrial

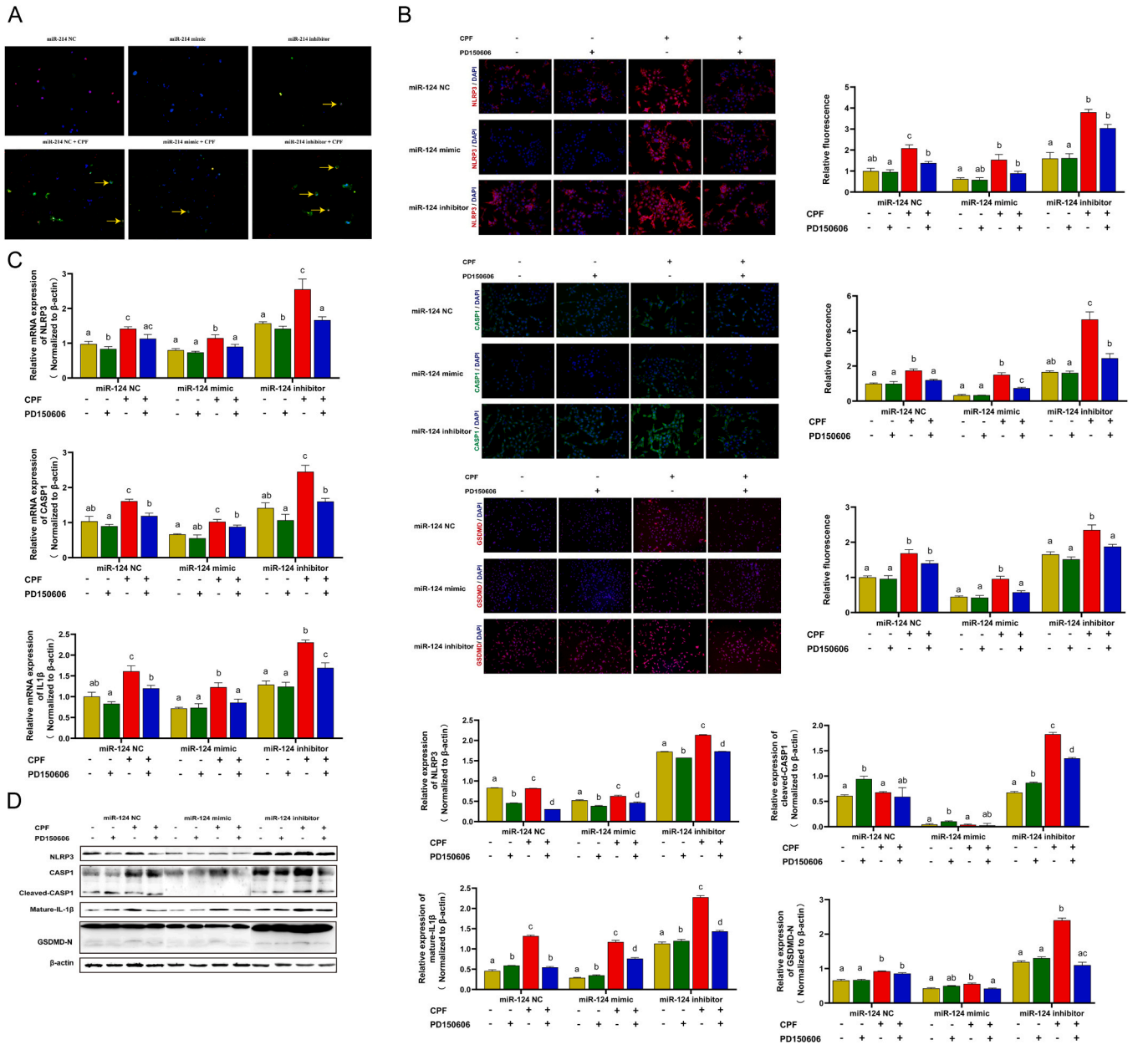

Fig. 3. miR-124-3p targets CAPN1 to regulate CPF-induced pyroptosis. (A) The pyroptotic cells (yellow arrow). The transfected cells were treated with or without 7 μM CPF, and Hoechst (blue) was loaded into the cells for 30 min in an ice bath. Then, Annexin V-FITC (green) and PI (red) were applied to detect pyroptosis, which is characterized by extensive membrane bubbling. The obvious green blebs (yellow arrow) were more distinct after CPF exposure. (B) Immunofluorescence staining of the cells with NLRP3 antibody (red), CASP1 (green), GSDMD (red) and DAPI (blue). The fluorescence of the cells was measured from three randomly chosen fields of view and normalized to the fluorescence of the miR-124 NC cell model without CPF and PD150606 treatments. (C) The mRNA expression of NLRP3, CASP1 and IL1β in each group. (D) The protein levels of NLRP3, cleaved CASP1, mature IL1β and GSDMD N-terminal (GSDMD-N) in each group. The data were analysed by two-way ANOVA, and different superscript letters display statistically significant differences ($P < 0.05$).

dysfunction, resulting in ROS generation via the miR-124-3p/CAPN1 axis.

3.3. CPF induced pyroptosis by activating CAPN1

Pyroptotic cells are characterized by membrane blebbing and ballooning and eventual membrane integrity loss (Fink and Cookson, 2005). To further confirm whether CPF can induce cell pyroptosis, pyroptosis alterations and the expression of pyroptosis-related indicators were detected in the present study. Annexin V-FITC, PI and Hoechst staining were performed to stain pyroptotic cells, as shown in Fig. 3A. Obvious green membrane blebbing, a characteristic of pyroptotic cells, was seen after CPF treatment. There was less cell death in the mimic group than in the inhibitor group, which indicated that CPF induces EPC cell pyroptosis by regulating miR-124-3p. A previous study demonstrated that activation of the NLRP3 inflammasome is regulated by mitochondrial oxidative stress, resulting in proptosis in human keratinocyte cells (Jang et al., 2015). Immunofluorescence was used to examine the synthesis of NLRP3, CASP1 and GSDMD, as shown in Fig. 3B. Based on these results, CPF exposure significantly activated NLRP3, CASP1 and GSDMD, which means that CPF recruits NLRP3 and CASP1 to activate the NLRP3 inflammasome pathway. Additionally, the CAPN1 inhibitor blocked the effects of CPF on the NLRP3 inflammasome pathway, as the NLRP3, CASP1 and GSDMD expression levels were moderated after supplementation with PD150606. Consistent with expectations, a higher expression level of pyroptosis-related genes was observed in the miR-124 inhibitor groups than in the miR-124 mimic groups, which showed that miR-124/CAPN1 is associated with CPF-induced pyroptosis via the NLRP3 pathway. Therefore, qRT-PCR and western blot analysis were applied to quantify the expression of NLRP3 pathway genes in this study, as shown in Fig. 3C-D. We found that the expression levels of NLRP3, cleaved CASP1, mature IL1β and GSDMD N-terminal (GSDMD-N) were significantly ($P < 0.05$) elevated after CPF treatment and that these effects were blocked by the CAPN1 inhibitor. These results suggested that CPF induced pyroptosis via activation of CAPN1.

4. Discussion

CPF, as an environmental contaminate, threatens the population of common carp (*Cyprinus carpio* L.), due to its effective induction of inflammatory diseases (Altun et al., 2017). Kianpour et al. (2021) reported that CPF exposure induced rat hepatic and pulmonary inflammatory damage. Hirani et al. (2007) indicated that the CPF-activated proinflammatory pathway may be dominant in neurotoxicity in mice. Zhang et al. (2017b) revealed that CPF-triggered zebrafish liver lesions depend on the pathology analysis. Pyroptosis is a novel inflammatory form of programmed cell death and has been reported to contribute to an extensive inflammatory response, which is associated with improper injury repair of tissues and organs and eventually causes inflammatory disease (Hu et al., 2010; Lamkanfi and Dixit, 2012; Zaki et al., 2011). The aim of this study was to assess whether CPF exposure could elicit EPC cell pyroptotic death, and the potential signalling mechanism was found to be accompanied by cell pyroptosis. The present study results demonstrated that pyroptosis occurred in CPF-exposed EPC cells, and miR-124-3p expression was restrained and resulted in amplified expression of CAPN1 due to target regulatory relationships between the two. The depletion of MMP, polarization of mitochondrial fission (DRP1 and fusion (OPA1), augmented ROS generation, and reinforced expression of NLRP3, CASP1, IL1β and GSDMD indicated malfunctioning mitochondria, and the canonical NLRP3/CASP1 pathway was involved in CPF-induced pyroptosis.

Many researchers have attempted to understand and alleviate CPF-induced cytotoxicity by regulating miRNAs, such as Zhao et al. (2019), who reported that miR-181 is associated with CPF-induced human neuroblastoma cell pyroptosis. Liu et al. (2019) found that miR-731 and miR-2188 regulate CPF-induced head kidney damage in common carp. Additionally, Zhang et al. (2019) reported that miR-19a contributes to CPF-mediated apoptosis and autophagy in common carp. Accordingly, we designed miRNAs and targeted mRNAs that modulated CPF-mediated cell pyroptosis. The recent literature has reported that miR-124-3p regulates pyroptosis in trophoblast cells (Tao et al., 2020) and pulmonary arterial smooth muscle cells (Jiang et al., 2021). In addition, the highly conserved binding sites of miR-124 and CAPN1 have been demonstrated in various cell models (Angelopoulou et al., 2019; Kanagaraj et al., 2014; Zhou et al., 2019). Based on the prediction of TargetScan (http://www.targetscan.org/fish_62/), miR-124 families are highly conserved across most fish. In this study, we initially validated the miR-124-3p binding site in nucleotides 30–36 and 63–69 of the CAPN1 3'-UTR by double luciferase assays, which verified that miR-124-3p modulates CAPN1 in EPC cells and suppresses miR-124-3p expression to increase CAPN1 expression in CPF-exposed EPC cells. While the mechanism of the CPF effects on miR-124-3p expression are still obscure, we expect to confirm whether CPF modulates miR-124 biogenesis by direct binding or whether other modulators are involved, and an in vivo validation experiment of the binding relationship is necessary.

Numerous diseases associated with CAPN activity alterations support the elevation of ROS levels and the resulting increase in oxidative stress (Clement, 2014; Randriamboavonjy et al., 2019; Valko et al., 2006). Chen et al. (2014) reported that CAPNs participate in ROS generation. Mitochondria are considered the primary source of ROS generation mediated by CAPN (Randriamboavonjy et al., 2019). OPA1, as the mitochondrial inner membrane GTPase, has been reported to be targeted by CAPN1 and contribute to mitochondrial fragmentation (Jahani-Asl et al., 2011). Cao et al. (2019) reported that mitochondrial CAPN1 enhancement disrupts ATP synthesis, promotes superoxide generation and mitochondrial permeability transition pore (mPTP) opening, and this results in cardiomyocyte death. Guan et al. (2019) proved that activation of CAPN1 caused an increase in mitochondrial fission and inhibited fusion. Additionally, Angelopoulou et al. (2019) clarified that miR-124 targets CAPN1 and regulates mitochondrial dysfunction and cell survival. The results of this study showed that mitochondrial dysfunction mediated by CPF exposure was associated with MMP depletion and increased mitochondrial fission rather than fusion. In comparison with the miR-124 inhibitor groups, the cells in the miR-124 mimic groups exhibited better mitochondrial functional status, indicating that the miR-124-3p mimic-restrained CAPN1 expression results in less mitochondrial damage. CAPN1 translocates from the cytoplasm to mitochondria due to hyperhomocysteinemia-induced calcium flux elevation and increases ROS generation, thereby contributing to mitochondrial dysfunction and cell death (Moshal et al., 2006; Papatheodorou and Weiss, 2007). Wiegman et al. (2015) reported that mitochondrial dysfunction is accompanied by upregulation of mitochondrial ROS in patients with chronic obstructive pulmonary disease. The results of this study also demonstrated that CPF-induced mitochondrial dysfunction results in mitochondrial ROS elevation and also affects cytoplasmic ROS levels. Simultaneously, several studies have explored the role of miR-124 in CAPN expression associated with ROS (Cai et al., 2016; Hu et al., 2017; Kanagaraj et al., 2014). Kanagaraj et al. (2014) found that miR-124 knockdown elevated ROS production by interacting with CAPN1. Our results are consistent with previous studies, and enhanced ROS generation was detected in the miR-124 inhibitor groups rather than the mimic groups, which means that CAPN1 activation promotes mitochondrial dysfunction and this results in ROS level elevation.

Inflammasomes play a crucial role in the intrinsic immune system as the first line of host defence (Zheng and Kanneganti, 2020) and they are assembled by sensor molecules, such as the NLR family. NLRP3, as an inflammasome sensor, interacts with apoptosis-associated speck-like protein (ASC) as an adapter molecule and this results in the recruitment and activation of CASP1. Activated CASP1 triggers cleavage of pro-IL1β

and pro-IL18 to establish proinflammatory responses (Man and Kanneganti, 2016; Schroder and Tschopp, 2010) and frees the N-terminus of the pore-forming protein GSDMD, causing pore structure assembly in the cell membrane and mediating pyroptosis (He et al., 2015; Kayagaki et al., 2015; Shi et al., 2015). Zhou et al. (2011) found that mitochondrial ROS are produced by respiratory chain inhibition, which eventually activates the NLRP3 inflammasome. Gross et al. (2011) revealed that the NLRP3 inflammasome is triggered by ROS accumulation, which was generated by the mitochondria. Han et al. (2018) reported that excessive mito-ROS production upregulates the expression of NLRP3 and IL1β in patients with diabetic nephropathy. Jia et al. (2020) demonstrated that mito-ROS upregulates oxidized mitochondrial DNA and activates the NLRP3 inflammasome in arsenic-exposed hepatic insulin resistance. In this study, we found that the proportion of pyroptotic cells increased under CPF exposure, as characterized by extensive membrane bubbling. More pyroptotic cells appeared in the miR-124 inhibitor group than in the mimic group, which further confirmed that miR-124 targeting CAPN1 participates in CPF-induced pyroptosis. The expression levels of NLRP3, CASP1, IL1β and GSDMD were prominently increased under CPF exposure and in the miR-124 inhibitor groups, indicating that mitochondrial ROS elevation evokes the canonical NLRP3 inflammasome pathway and induces cell pyroptosis. Consistent results have been obtained in numerous toxicant studies. Wu et al. (2018) confirming that nicotine triggers endothelial cell pyroptosis via the ROS-NLRP3 inflammasome and this results in atherosclerosis. The ROS-dependent NLRP3 inflammasome results in pyroptosis in lipopolysaccharide-stimulated cardiomyocytes (Li et al., 2019). LPS enhanced the expression of Never in Mitosis A-related kinase 7 (NEK7), which evokes pyroptosis by interacting with NLRP3 and is involved in inflammatory bowel disease (Chen et al., 2019). Additionally, the occurrence of NLRP3 inflammasome-mediated pyroptosis in doxorubicin-treated heart tissue was detected by Zeng et al. (2020). However, in vivo experiments were not performed in this study. We aim to investigate the toxicity of CPF in common carp and the relationship of miR-124-3p and CAPN1, which will be the main focus of future studies.

5. Conclusion

Taken together, the present study primarily identified a targeted binding relationship between miR-124-3p and CAPN1 in EPC cells and demonstrated that pyroptotic death occurred in CPF-exposed EPC cells, which was accompanied by restrained miR-124-3p expression and elevated CAPN1 expression to trigger mitochondrial dysfunction, ROS overproduction and NLRP3/IL1β/GSDMD pathway activation. All of the results indicate that CPF-triggered EPC cell pyroptosis by regulating the miR-124-3p/CAPN1 axis. This study not only provides new information for CPF cytotoxicity studies but also supports a novel academic basis for the exploration of miRNA and its target protein response to water contaminants.

CRediT authorship contribution statement

Zhiying Miao: Conceptualization, Data curation, Formal analysis, Investigation, Writing – original draft. **Zhiruo Miao:** Investigation, Data curation, Visualization, Writing – editing. **Xiaohua Teng:** Supervision, Funding acquisition, Writing – review & editing. **Shiwen Xu:** Supervision, Funding acquisition, Writing – review & editing.

Declaration of Competing Interest

The authors declare that they have no known competing financial interests or personal relationships that could have appeared to influence the work reported in this study.

Acknowledgement

This work was supported by National Natural Science Foundation of China (No. 31972612) and Hualong Feed Research Collaboration of China (No. 860035). The funding body played no role in the design of the study and collection, analysis, and interpretation of data and in writing the manuscript.

References

Albasher, G., Albrahim, T., Alsultan, N., Alfaraj, S., Alharthi, M.S., Kassab, R.B., Abdel Moneim, A.E., 2020. Red beetroot extract mitigates chlorpyrifos-induced reprotoxicity associated with oxidative stress, inflammation, and apoptosis in rats. Environ. Sci. Pollut. Res Int 27, 3979–3991. https://doi.org/10.1007/s11356-019-07009-6.

AlKahtane, A.A., Ghanem, E., Bungau, S.G., Alarifi, S., Ali, D., AlBasher, G., Alkahtani, S., Aleya, L., Abdel-Daim, M.M., 2020. Carnosic acid alleviates chlorpyrifos-induced oxidative stress and inflammation in mice cerebral and ocular tissues. Environ. Sci. Pollut. Res Int 27, 11663–11670. https://doi.org/10.1007/s11356-020-07736-1.

Altun, S., Ozdemir, S., Arslan, H., 2017. Histopathological effects, responses of oxidative stress, inflammation, apoptosis biomarkers and alteration of gene expressions related to apoptosis, oxidative stress, and reproductive system in chlorpyrifos-exposed common carp (Cyprinus carpio l.). Environ. Pollut. 230, 432–443. https://doi.org/10.1016/j.envpol.2017.06.085.

Angelopoulou, E., Paudel, Y.N., Piperi, C., 2019. Mir-124 and parkinson's disease: A biomarker with therapeutic potential. Pharm. Res 150, 104515. https://doi.org/10.1016/j.phrs.2019.104515.

Bergsbaken, T., Fink, S.L., Cookson, B.T., 2009. Pyroptosis: host cell death and inflammation. Nat. Rev. Microbiol 7, 99–109. https://doi.org/10.1038/nrmicro2070.

Broz, P., Pelegrin, P., Shao, F., 2020. The gasdermins, a protein family executing cell death and inflammation. Nat. Rev. Immunol. 20, 143–157. https://doi.org/10.1038/s41577-019-0228-2.

Cai, J.J., Qi, Z.X., Chen, L.C., Yao, Y., Gong, Y., Mao, Y., 2016. Mir-124 suppresses the migration and invasion of glioma cells in vitro via capn4. Oncol. Rep. 35, 284–290. https://doi.org/10.3892/or.2015.4355.

Cao, T., Fan, S., Zheng, D., Wang, G., Yu, Y., Chen, R., Song, L.S., Fan, G.C., Zhang, Z., Peng, T., 2019. Increased calpain-1 in mitochondria induces dilated heart failure in mice: role of mitochondrial superoxide anion. Basic Res Cardiol. 114, 17. https://doi.org/10.1007/s00395-019-0726-1.

Chen, B., Zhao, Q., Ni, R., Tang, F., Shan, L., Cepinskas, I., Cepinskas, G., Wang, W., Schiller, P.W., Peng, T., 2014. Inhibition of calpain reduces oxidative stress and attenuates endothelial dysfunction in diabetes. Cardiovasc Diabetol. 13, 88. https://doi.org/10.1186/1475-2840-13-88.

Chen, X., Liu, G., Yuan, Y., Wu, G., Wang, S., Yuan, L., 2019. NEK7 interacts with NLRP3 to modulate the pyroptosis in inflammatory bowel disease via NF-κB signaling. Cell Death Dis. 10, 906. https://doi.org/10.1038/s41419-019-2157-1.

Clement, M.V., 2014. Nitric oxide-based protein modification: Formation and site-specificity of protein s-nitrosylation: Could protein s-nitrosylation be the unifying oxidative modification to explain the cellular signaling activity of superoxide and hydrogen peroxide? Free Radic. Biol. Med 75 Suppl 1 (Suppl 1), 14. https://doi.org/10.1016/j.freeradbiomed.2014.10.586.

Cowgill, U.M., Gowland, R.T., Ramirez, C.A., Fernandez, V., 1991. The history of a chlorpyrifos spill: cartagena, colombia. Environ. Int. 17, 61–71. https://doi.org/10.1016/0160-4120(91)90338-Q.

Dawood, M.A.O., El-Salam Metwally, A., Elkomy, A.H., Gewaily, M.S., Abdo, S.E., Abdel-Razek, M.A.S., Soliman, A.A., Amer, A.A., Abdel-Razik, N.I., Abdel-Latif, H.M.R., Paray, B.A., 2020. The impact of menthol essential oil against inflammation, immunosuppression, and histopathological alterations induced by chlorpyrifos in nile tilapia. Fish. Shellfish Immunol. 102, 316–325. https://doi.org/10.1016/j.fsi.2020.04.059.

EPA 2000. Human risk assessment: Chlorpyrifos. Us environ, protection agency.

Fink, S.L., Cookson, B.T., 2005. Apoptosis, pyroptosis, and necrosis: Mechanistic description of dead and dying eukaryotic cells. Infect. Immun. 73, 1907–1916. https://doi.org/10.1128/IAI.73.4.1907-1916.2005.

Goll, D.E., Thompson, V.F., Li, H., Wei, W., Cong, J., 2003. The calpain system. Physiol. Rev. 83, 731–801. https://doi.org/10.1152/physrev.00029.2002.

Gorrini, C., Harris, I.S., Mak, T.W., 2013. Modulation of oxidative stress as an anticancer strategy. Nat. Rev. Drug Disco 12, 931–947. https://doi.org/10.1038/nrd4002.

Gross, O., Thomas, C.J., Guarda, G., Tschopp, J., 2011. The inflammasome: An integrated view. Immunol. Rev. 243, 136–151. https://doi.org/10.1111/j.1600-065X.2011.01046.x.

Guan, L., Che, Z., Meng, X., Yu, Y., Li, M., Yu, Z., Shi, H., Yang, D., Yu, M., 2019. Mcu up-regulation contributes to myocardial ischemia-reperfusion injury through calpain/opa-1-mediated mitochondrial fusion/mitophagy inhibition. J. Cell Mol. Med 23, 7830–7843. https://doi.org/10.1111/jcmm.14662.

Han, Y., Xu, X., Tang, C., Gao, P., Chen, X., Xiong, X., Yang, M., Yang, S., Zhu, X., Yuan, S., Liu, F., Xiao, L., Kanwar, Y.S., Sun, L., 2018. Reactive oxygen species promote tubular injury in diabetic nephropathy: The role of the mitochondrial ros-txnip-nlrp3 biological axis. Redox Biol. 16, 32–46. https://doi.org/10.1016/j.redox.2018.02.013.

He, W.T., Wan, H., Hu, L., Chen, P., Wang, X., Huang, Z., Yang, Z.H., Zhong, C.Q., Han, J., 2015. Gasdermin d is an executor of pyroptosis and required for interleukin-1beta secretion. Cell Res. 25, 1285–1298. https://doi.org/10.1038/cr.2015.139.
Hirani, A., Lee, W.H., Kang, S.K., Ehrich, M., Lee, Y.W., 2007. Chlorpyrifos induces pro-inflammatory environment in discrete regions of mouse brain. Faseb J. 21, A988.
Hu, B., Elinav, E., Huber, S., Booth, C.J., Strowig, T., Jin, C., Eisenbarth, S.C., Flavell, R. A., 2010. Inflammation-induced tumorigenesis in the colon is regulated by caspase-1 and nlrc4. Proc. Natl. Acad. Sci. U.S.A. 107, 21635–21640. https://doi.org/10.1073/pnas.1016814108.
Hu, H., Wang, G., Li, C., 2017. Mir-124 suppresses proliferation and invasion of nasopharyngeal carcinoma cells through the wnt/beta-catenin signaling pathway by targeting capn4. Onco Targets Ther. 10, 2711–2720. https://doi.org/10.2147/OTT.S135563.
Huang, X., Cui, H., Duan, W., 2020. Ecotoxicity of chlorpyrifos to aquatic organisms: a review. Ecotoxicol. Environ. Saf. 200, 110731 https://doi.org/10.1016/j.ecoenv.2020.110731.
Jahani-Asl, A., Pilon-Larose, K., Xu, W., MacLaurin, J.G., Park, D.S., McBride, H.M., Slack, R.S., 2011. The mitochondrial inner membrane gtpase, optic atrophy 1 (opa1), restores mitochondrial morphology and promotes neuronal survival following excitotoxicity. J. Biol. Chem. 286, 4772–4782. https://doi.org/10.1074/jbc.M110.167155.
Jang, Y., Lee, A.Y., Jeong, S.H., Park, K.H., Paik, M.K., Cho, N.J., Kim, J.E., Cho, M.H., 2015. Chlorpyrifos induces nlrp3 inflammasome and pyroptosis/apoptosis via mitochondrial oxidative stress in human keratinocyte hacat cells. Toxicology 338, 37–46. https://doi.org/10.1016/j.tox.2015.09.006.
Jia, X., Qiu, T., Yao, X., Jiang, L., Wang, N., Wei, S., Tao, Y., Pei, P., Wang, Z., Zhang, J., Zhu, Y., Yang, G., Liu, X., Liu, S., Sun, X., 2020. Arsenic induces hepatic insulin resistance via mtros-nlrp3 inflammasome pathway. J. Hazard Mater. 399, 123034 https://doi.org/10.1016/j.jhazmat.2020.123034.
Jiang, Y., Liu, H., Yu, H., Zhou, Y., Zhang, J., Xin, W., Li, Y., He, S., Ma, C., Zheng, X., Zhang, L., Zhao, X., Wu, B., Jiang, C., Zhu, D., 2021. Circular rna calm4 regulates hypoxia-induced pulmonary arterial smooth muscle cells pyroptosis via the circ-calm4/mir-124-3p/pdcd6 axis. Arterioscler. Thromb. Vasc. Biol. 41, 1675–1693. https://doi.org/10.1161/ATVBAHA.120.315525.
Kanagaraj, N., Beiping, H., Dheen, S.T., Tay, S.S., 2014. Downregulation of mir-124 in mptp-treated mouse model of Parkinson's disease and mpp iodide-treated mn9d cells modulates the expression of the calpain/cdk5 pathway proteins. Neuroscience 272, 167–179. https://doi.org/10.1016/j.neuroscience.2014.04.039.
Karbalaei, S., Hanachi, P., Rafiee, G., Seifori, P., Walker, T.R., 2021. Toxicity of polystyrene microplastics on juvenile Oncorhynchus mykiss (rainbow trout) after individual and combined exposure with chlorpyrifos. J. Hazard Mater. 403, 123980 https://doi.org/10.1016/j.jhazmat.2020.123980.
Kayagaki, N., Stowe, I.B., Lee, B.L., O'Rourke, K., Anderson, K., Warming, S., Cuellar, T., Haley, B., Roose-Girma, M., Phung, Q.T., Liu, P.S., Lill, J.R., Li, H., Wu, J., Kummerfeld, S., Zhang, J., Lee, W.P., Snipas, S.J., Salvesen, G.S., Morris, L.X., Fitzgerald, L., Zhang, Y., Bertram, E.M., Goodnow, C.C., Dixit, V.M., 2015. Caspase-11 cleaves gasdermin d for non-canonical inflammasome signalling. Nature 526, 666–671. https://doi.org/10.1038/nature15541.
Kianpour, F., Mohseni, M., Beigmohamadi, M., Yazdinezhad, A., Ramazani, A., Hosseini, M.J., Sharafi, A., 2021. The protective effects of ziziphora tenuior l. Against chlorpyrifos induced toxicity: Involvement of inflammatory and cell death signaling pathway. J. Ethnopharmacol. 272, 113959 https://doi.org/10.1016/j.jep.2021.113959.
Lamkanfi, M., Dixit, V.M., 2012. Inflammasomes and their roles in health and disease. Annu Rev. Cell Dev. Biol. 28, 137–161. https://doi.org/10.1146/annurev-cellbio-101011-155745.
Li, N., Zhou, H., Wu, H., Wu, Q., Duan, M., Deng, W., Tang, Q., 2019. Sting-irf3 contributes to lipopolysaccharide-induced cardiac dysfunction, inflammation, apoptosis and pyroptosis by activating nlrp3. Redox Biol. 24, 101215 https://doi.org/10.1016/j.redox.2019.101215.
Liang, Y., Zhan, J., Liu, D., Luo, M., Han, J., Liu, X., Liu, C., Cheng, Z., Zhou, Z., Wang, P., 2019. Organophosphorus pesticide chlorpyrifos intake promotes obesity and insulin resistance through impacting gut and gut microbiota. Microbiome 7, 19. https://doi.org/10.1186/s40168-019-0635-4.
Liao, L., Dai, X., Fan, F., Ye, Y., Chen, F., Wu, Z., Lu, X., Wei, Q., Chen, J., Yan, Y., 2017. Determination of chlorpyrifos in human blood by gas chromatography-mass spectrometry. J. Forensic Sci. Med. 3, 22. https://doi.org/10.4103/jfsm.jfsm_2_17.
Liu, Q., Yang, J., Gong, Y., Cai, J., Zhang, Z., 2019. Role of mir-731 and mir-2188-3p in mediating chlorpyrifos induced head kidney injury in common carp via targeting tlr and apoptosis pathways. Aquat. Toxicol. 215, 105286 https://doi.org/10.1016/j.aquatox.2019.105286.
Luo, T., Yue, R., Hu, H., Zhou, Z., Yiu, K.H., Zhang, S., Xu, L., Li, K., Yu, Z., 2015. Pd150606 protects against ischemia/reperfusion injury by preventing mu-calpain-induced mitochondrial apoptosis. Arch. Biochem Biophys. 586, 1–9. https://doi.org/10.1016/j.abb.2015.06.005.
Man, S.M., Kanneganti, T.D., 2016. Converging roles of caspases in inflammasome activation, cell death and innate immunity. Nat. Rev. Immunol. 16, 7–21. https://doi.org/10.1038/nri.2015.7.
Moshal, K.S., Singh, M., Sen, U., Rosenberger, D.S., Henderson, B., Tyagi, N., Zhang, H., Tyagi, S.C., 2006. Homocysteine-mediated activation and mitochondrial translocation of calpain regulates mmp-9 in mvec. Am. J. Physiol. Heart Circ. Physiol. 291, H2825–2835. https://doi.org/10.1152/ajpheart.00377.2006.
Naime, A.A., Lopes, M.W., Colle, D., Dafre, A.L., Sunol, C., da Rocha, J.B.T., Aschner, M., Leal, R.B., Farina, M., 2020. Glutathione in chlorpyrifos-and chlorpyrifos-oxon-induced toxicity: a comparative study focused on non-cholinergic toxicity in ht22 cells. Neurotox. Res. 38, 603–610. https://doi.org/10.1007/s12640-020-00254-5.
Ojha, A., Yaduvanshi, S.K., Pant, S.C., Lomash, V., Srivastava, N., 2013. Evaluation of DNA damage and cytotoxicity induced by three commonly used organophosphate pesticides individually and in mixture, in rat tissues. Environ. Toxicol. 28, 543–552. https://doi.org/10.1002/tox.20748.
Osellame, L.D., Rahim, A.A., Hargreaves, I.P., Gegg, M.E., Richard-Londt, A., Brandner, S., Waddington, S.N., Schapira, A.H.V., Duchen, M.R., 2013. Mitochondria and quality control defects in a mouse model of gaucher disease–links to Parkinson's disease. Cell Metab. 17, 941–953. https://doi.org/10.1016/j.cmet.2013.04.014.
Papatheodorou, L., Weiss, N., 2007. Vascular oxidant stress and inflammation in hyperhomocysteinemia. Antioxid. Redox Signal 9, 1941–1958. https://doi.org/10.1089/ars.2007.1750.
Pesticide Data Programs of USA, 2016. www.ams.usda.gov/pdp.
Pundir, C.S., Malik, A., Preety, 2019. Bio-sensing of organophosphorus pesticides: a review. Biosens. Bioelectron. 140, 111348 https://doi.org/10.1016/j.bios.2019.111348.
Randriamboavonjy, V., Kyselova, A., Fleming, I., 2019. Redox regulation of calpains: Consequences on vascular function. Antioxid. Redox Signal 30, 1011–1026. https://doi.org/10.1089/ars.2018.7607.
Reuter, S., Gupta, S.C., Chaturvedi, M.M., Aggarwal, B.B., 2010. Oxidative stress, inflammation, and cancer: How are they linked? Free Radic. Biol. Med 49, 1603–1616. https://doi.org/10.1016/j.freeradbiomed.2010.09.006.
Schroder, K., Tschopp, J., 2010. The inflammasomes. Cell 140, 821–832. https://doi.org/10.1016/j.cell.2010.01.040.
Shi, J., Zhao, Y., Wang, K., Shi, X., Wang, Y., Huang, H., Zhuang, Y., Cai, T., Wang, F., Shao, F., 2015. Cleavage of gsdmd by inflammatory caspases determines pyroptotic cell death. Nature 526, 660–665. https://doi.org/10.1038/nature15514.
Song, N., Li, X., Cui, Y., Zhang, T., Xu, S., Li, S., 2021. Hydrogen sulfide exposure induces pyroptosis in the trachea of broilers via the regulatory effect of circrna-17828/mir-6631-5p/dusp6 crosstalk on ros production. J. Hazard Mater. 418, 126172 https://doi.org/10.1016/j.jhazmat.2021.126172.
Storr, S.J., Carragher, N.O., Frame, M.C., Parr, T., Martin, S.G., 2011. The calpain system and cancer. Nat. Rev. Cancer 11, 364–374. https://doi.org/10.1038/nrc3050.
Tangmansakulchai, K., Abubakar, Z., Kitiyanant, N., Suwanjang, W., Leepiyasakulchai, C., Govitrapong, P., Chetsawang, B., 2016. Calpastatin overexpression reduces oxidative stress-induced mitochondrial impairment and cell death in human neuroblastoma sh-sy5y cells by decreasing calpain and calcineurin activation, induction of mitochondrial fission and destruction of mitochondrial fusion. Mitochondrion 30, 151–161. https://doi.org/10.1016/j.mito.2016.07.009.
Tao, J., Xia, L.Z., Liang, L., Chen, Y., Wei, D., Meng, J., Wu, S., Wang, Z., 2020. Mir-124-3p promotes trophoblast cell htr-8/svneo pyroptosis by targeting. Placent. Growth Factor. Placenta 101, 176–184. https://doi.org/10.1016/j.placenta.2020.08.011.
Tong, M., Zablocki, D., Sadoshima, J., 2020. The role of drp1 in mitophagy and cell death in the heart. J. Mol. Cell Cardiol. 142, 138–145. https://doi.org/10.1016/j.yjmcc.2020.04.015.
Valko, M., Rhodes, C.J., Moncol, J., Izakovic, M., Mazur, M., 2006. Free radicals, metals and antioxidants in oxidative stress-induced cancer. Chem. Biol. Inter. 160, 1–40. https://doi.org/10.1016/j.cbi.2005.12.009.
Weis, G.C.C., Assmann, C.E., Mostardeiro, V.B., Alves, A.O., da Rosa, J.R., Pillat, M.M., de Andrade, C.M., Schetinger, M.R.C., Morsch, V.M.M., da Cruz, I.B.M., Costabeber, I.H., 2021. Chlorpyrifos pesticide promotes oxidative stress and increases inflammatory states in bv-2 microglial cells: A role in neuroinflammation. Chemosphere 278, 130417. https://doi.org/10.1016/j.chemosphere.2021.130417.
Wiegman, C.H., Michaeloudes, C., Haji, G., Narang, P., Clarke, C.J., Russell, K.E., Bao, W., Pavlidis, S., Barnes, P.J., Kanerva, J., Bittner, A., Rao, N., Murphy, M.P., Kirkham, P.A., Chung, K.F., Adcock, I.M., Copdmap, 2015. Oxidative stress-induced mitochondrial dysfunction drives inflammation and airway smooth muscle remodeling in patients with chronic obstructive pulmonary disease. J. Allergy Clin. Immunol. 136, 769–780. https://doi.org/10.1016/j.jaci.2015.01.046.
Williams, W.M., Giddings, J.M., Purdy, J., Solomon, K.R., Giesy, J.P., 2014. Exposures of aquatic organisms to the organophosphorus insecticide, chlorpyrifos resulting from use in the united states. Rev. Environ. Contam. Toxicol. 231, 77–117. https://doi.org/10.1007/978-3-319-03865-0_4.
Wu, X., Zhang, H., Qi, W., Zhang, Y., Li, J., Li, Z., Lin, Y., Bai, X., Liu, X., Chen, X., Yang, H., Xu, C., Zhang, Y., Yang, B., 2018. Nicotine promotes atherosclerosis via ros-nlrp3-mediated endothelial cell pyroptosis. Cell Death Dis. 9, 171. https://doi.org/10.1038/s41419-017-0257-3.
Yamada, S., Kubo, Y., Yamazaki, D., Sekino, Y., Kanda, Y., 2017. Chlorpyrifos inhibits neural induction via mfn1-mediated mitochondrial dysfunction in human induced pluripotent stem cells. Sci. Rep. 7, 40925. https://doi.org/10.1038/srep40925.
Yu, Y., Shi, H., Yu, Y., Liu, M., Li, M., Liu, X., Wang, Y., Chen, R., 2020. Inhibition of calpain alleviates coxsackievirus b3-induced myocarditis through suppressing the canonical nlrp3 inflammasome/caspase-1-mediated and noncanonical caspase-11-mediated pyroptosis pathways. Am. J. Transl. Res 12, 1954–1964.
Yue, R.C., Lu, S.Z., Luo, Y., Wang, T., Liang, H., Zeng, J., Liu, J., Hu, H.X., 2019. Calpain silencing alleviates myocardial ischemia-reperfusion injury through the nlrp3/asc/caspase-1 axis in mice. Life Sci. 233, 116631 https://doi.org/10.1016/j.lfs.2019.116631.
Zaki, M.H., Lamkanfi, M., Kanneganti, T.D., 2011. The nlrp3 inflammasome: Contributions to intestinal homeostasis. Trends Immunol. 32, 171–179. https://doi.org/10.1016/j.it.2011.02.002.
Zeng, C., Duan, F., Hu, J., Luo, B., Huang, B., Lou, X., Sun, X., Li, H., Zhang, X., Yin, S., Tan, H., 2020. Nlrp3 inflammasome-mediated pyroptosis contributes to the pathogenesis of non-ischemic dilated cardiomyopathy. Redox Biol. 34, 101523 https://doi.org/10.1016/j.redox.2020.101523.
Zhang, C., Lin, T., Nie, G., Hu, R., Pi, S., Wei, Z., Wang, C., Xing, C., Hu, G., 2021. Cadmium and molybdenum co-induce pyroptosis via ros/pten/pi3k/akt axis in duck

renal tubular epithelial cells. Environ. Pollut. 272, 116403 https://doi.org/10.1016/j.envpol.2020.116403.

Zhang, J., Liu, L., Ren, L., Feng, W., Lv, P., Wu, W., Yan, Y., 2017b. The single and joint toxicity effects of chlorpyrifos and beta-cypermethrin in zebrafish (Danio rerio) early life stages. J. Hazard Mater. 334, 121–131. https://doi.org/10.1016/j.jhazmat.2017.03.055.

Zhang, Q., Zheng, S., Wang, S., Wang, W., Xing, H., Xu, S., 2019. Chlorpyrifos induced oxidative stress to promote apoptosis and autophagy through the regulation of mir-19a-ampk axis in common carp. Fish. Shellfish Immunol. 93, 1093–1099. https://doi.org/10.1016/j.fsi.2019.07.022.

Zhang, Y., Rong, H., Zhang, F.X., Wu, K., Mu, L., Meng, J., Xiao, B., Zamponi, G.W., Shi, Y., 2018. A membrane potential- and calpain-dependent reversal of caspase-1 inhibition regulates canonical nlrp3 inflammasome. Cell Rep. 24, 2356–2369 e2355. https://doi.org/10.1016/j.celrep.2018.07.098.

Zhang, Z., Liu, Q., Cai, J., Yang, J., Shen, Q., Xu, S., 2017a. Chlorpyrifos exposure in common carp (Cyprinus carpio l.) leads to oxidative stress and immune responses. Fish. Shellfish Immunol. 67, 604–611. https://doi.org/10.1016/j.fsi.2017.06.048.

Zhao, M.W., Yang, P., Zhao, L.L., 2019. Chlorpyrifos activates cell pyroptosis and increases susceptibility on oxidative stress-induced toxicity by mir-181/sirt1/pgc-1alpha/nrf2 signaling pathway in human neuroblastoma sh-sy5y cells: implication for association between chlorpyrifos and parkinson's disease. Environ. Toxicol. 34, 699–707. https://doi.org/10.1002/tox.22736.

Zheng, M., Kanneganti, T.D., 2020. The regulation of the zbp1-nlrp3 inflammasome and its implications in pyroptosis, apoptosis, and necroptosis (panoptosis). Immunol. Rev. 297, 26–38. https://doi.org/10.1111/imr.12909.

Zhou, R., Yazdi, A.S., Menu, P., Tschopp, J., 2011. A role for mitochondria in nlrp3 inflammasome activation. Nature 469, 221–225. https://doi.org/10.1038/nature09663.

Zhou, Y., Deng, J., Chu, X., Zhao, Y., Guo, Y., 2019. Role of post-transcriptional control of calpain by mir-124-3p in the development of alzheimer's disease. J. Alzheimers Dis. 67, 571–581. https://doi.org/10.3233/JAD-181053.